Desalination and Water Treatment
www.deswater.com

doi: 10.5004/dwt.2021.27407

230 (2021) 288–297
August

Sulfonic modified mesoporous silica for the removal of cationic dyes

Ru Li*, Xin Huang, Yumeng Zhang

School of Resources and Civil Engineering, Northeastern University, 11 Wenhua Road, Heping District, Shenyang 110819, China, emails: liru@mail.neu.edu.cn (R. Li), 1870886@stu.neu.edu.cn (X. Huang), 1976204000@qq.com (Y. Zhang)

Received 23 February 2021; Accepted 12 May 2021

ABSTRACT

Sulfonic acid groups were employed to improve the adsorption capacity of MCM-41 for cationic dyes removal in the present study. Fourier transform infrared spectroscopy, thermogravimetric analysis, X-ray diffraction, transmission electron microscopy, energy dispersive X-ray spectroscopy assisted with scanning electron microscopy, and nitrogen adsorption–desorption were used to determine the differences between MCM-41 and sulfonic modified MCM-41 (S-MCM-41), and S-MCM-41 still possessed the ordered 2D hexagonal structure. Furthermore, experiments were carried out to explore the adsorption process of methylene blue (MB) on S-MCM-41 and to compare the adsorption capacity of S-MCM-41 with the capacity of MCM-41. The effect of pH values and adsorbent dose on the removal of MB were investigated, and S-MCM-41 can perform better at a pH value of 11 and adsorbent/adsorbate dose of 1.0 g/L. The pseudo-first-order and pseudo-second-order kinetic models were utilized to describe the adsorption process., and it fits better with the pseudo-first-order kinetic model (R^2 = 0.994). The adsorption isotherm was studied by the Langmuir model (R^2 = 0.995). Moreover, the regeneration study suggests S-MCM-41 can be easily recovered. S-MCM-41 possesses a high adsorption capacity of 593.22 mg/g while MCM-41 has a fine capacity of 463.23 mg/g, and therefore S-MCM-41 is a promising adsorbent for the removal of cationic dyes.

Keywords: Mesoporous silica; Modification; Sulfonic acid; Methylene blue; MCM-41

1. Introduction

Currently, more than one million types of dyes are employed in various walks of life and more than 900,000 tons was generated per year [1]. Aquatic life can be seriously poisoned by the dyes in the wastewater [2]. Therefore, many studies have been devoted to separating these pollutants from wastewater. Dyes in the wastewater must be separated and removed, even at a limited quantity due to its toxicity [3]. For example, methylene blue (MB) is frequently used in wood, cotton, and silk dying [4]. It will lead to health problems if inhaled or ingested [5]. Eosin Yellow is used for the Gram straining of the bacterial species and is well-applied in many industrial fields [6]. Eosin Yellow can damage human beings' eyes, skin, kidneys, liver, and lungs [7].

Generally, persistent and effective dyes are more preferred by manufacturers and consumers, and therefore the frequently used dyes are not easy to degrade. The efficiency of the biological degradation method for dye removal is limited, and the borderline products in this process are poisonous [8]. Hence, more eligible technologies need to be developed for dyes treatment.

Adsorption has been acknowledged as an economic and green way to remove dyes from wastewater [9]. Various adsorbents including activated carbons, zeolites, silica, clays, and bio-wastes for adsorption of different dyes have been fully studied [10–12]. Mesoporous silica with large surface area and pores has excellent performance on the adsorption of dyes [11]. Therefore, the next step of research should be modification of adsorbents to improve the adsorption capacity further.

* Corresponding author.

Most studies are focused on grafting amino-group onto mesoporous silica to improve the adsorption for cationic dyes [13–15], and other functional groups like ethenyl and carboxyl groups are also reported [16–18]. Apart from grafting organic functional groups, other modification methods including loading metallic oxides [19] and ultrasound treatment [20] are also investigated. From the above research, grafting functional groups can improve the adsorption capacity better than other methods. Therefore, more possible functional groups need to be discovered. In the present study, the potential of sulfonic groups grafted on mesoporous silica to adsorb dyes has been studied for the first time. Several research on grafting sulfonic groups for adsorption have been reported before [21,22]. Sulfonic groups have been recognized as promising functional groups for modification. Although sulfonic acids are strong acids, most kinds of dye wastewater are high in acidity or alkalinity, so the pH will be adjusted. Various characterization technologies have been employed to determine the changes after grafting sulfonic groups onto mesoporous silica MCM-41. Moreover, batch experiments were carried on to explore the adsorption performance of S-MCM-41.

2. Materials and methods

2.1. Chemicals and materials

The MCM-41 used in the present study was synthesized from boron waste as reported in our previous work. The other reagents such as hydrochloric acid (36.0% ~ 38.0%), sodium hydroxide (96.0%), sulfuric acid (95.0% ~ 98.0%), *n*-hexadecyltrimethyl ammonium bromide (CTAB, 99.0%), toluene, 3-mercaptopropyltrimethoxysilane, and H_2O_2 solution (30%) were analytical grade.

2.2. Synthesis of sulfonic modified MCM-41

Sulfonic groups were grafted onto the MCM-41 after the modification process which was reported elsewhere with change [23]. 1.5 g MCM-41 and 3.6 g 3-mercaptopropyltrimethoxysilane were added into 50 mL toluene. The mixture was stirred and refluxed at 110°C for 12 h. Then the solid was air-dried after filtering and washing by toluene. At the next stage, the solid was added into 40 mL 30% H2O2 solution and stirred at room temperature for 24 h. Before the resulting solid was added and stirred in 40 mL 0.2 M H2SO4 solution at room temperature overnight, it was filtered and washed with deionized water. The final sulfonic modified MCM-41 (S-MCM-41) was obtained by washing with deionized water and dried at 60°C.

2.3. Characterization

Fourier transform infrared (FTIR) spectroscopy and energy dispersive spectrometer were used to exam the sulfonic groups on the S-MCM-41. ThermoFisher Scientific Nicolet iS10 (Shanghai,China) was employed to perform the FTIR study, and energy dispersive X-ray spectroscopy (EDS) was performed combined with scanning electron microscopy (SEM). A thermogravimetric analysis (TGA) study was performed on NETZSCH STA449F3 at a heating rate of 23°C min^{-1}. X-ray diffraction (XRD) of Rigaku Smartlab was employed to determine the structure of modified MCM-41. XRD uses a Cu Kα radiation in the 2θ range of 1.5°–10° at an interval of 0.02° with a scanning rate of 1° min^{-1}. The morphology of S-MCM-41 was studied by SEM of ZEISS ULTRA PLUS and transmission electron microscopy (TEM) of FEI (G20). Before the SEM study, the samples of MCM-41 and S-MCM-41 have sprayed carbon. To carry on the TEM study, the samples were dispersed in absolute ethyl alcohol by an ultrasonic process. A glass rod was used to dip the turbid fluid onto carbon-coated copper grids before the TEM study commenced. Pore features of MCM-41 and S-MCM-41 were explored by nitrogen adsorption/desorption of Quantachrome (Autosorb-IQ-MP-C) at 77 K. A Zeta Plus potentiometer (Brookhaven, USA) was used to determine the zeta potential of S-MCM-41.

2.4. Adsorption of MB

The batch method was employed throughout the adsorption experiments. In every adsorption experiment, 100 mL conical flasks were used as reaction vessels. 20 mL MB solution and 20 mg adsorbents were added into a reaction vessel to explore their adsorption performance. All the flasks were shaken at 200 rpm in a gas bath shaker (TS-100B TENSUC, Shanghai). After the adsorption process, the mixture was centrifugated for 10 min at 10,000 rpm. The supernatant liquid was analyzed by a UV-vis spectrophotometer at 664 nm to determine the concentration of the remaining MB. The effect of pH value on the adsorption process was studied using 20 mg adsorbents to adsorb 500 mg/L MB solution for 60 min when the pH values varied from 2 to 12. The effect of adsorbent dose on the performance of S-MCM-41 was studied when the pH value was 11, and the adsorption process sustained 60 min. Q_e (mg/g) and the adsorbed percentage (A %) of dyes onto adsorbents were used to represent the adsorption capacity in the present study. They can be calculated by:

$$Q_e = \frac{\left(C_0 - C_e\right)V}{M} \tag{1}$$

$$A\% = \frac{\left(C_0 - C_e\right)}{C_0} \times 100 \tag{2}$$

where Q_e represents the adsorbed MB per gram of adsorbents when the adsorption process reached equilibrium. A% represents the percentage of removed dyes from raw wastewater. C_0 (mg/L) and C_e (mg/L) are the initial and equilibrium concentrations of the dyes in the wastewater, respectively. V (L) and M (g) represent the volume of MB and the mass of the adsorbents.

3. Results and discussion

3.1. Structure and morphology characterization

Fig. 1 presents the FT-IR results of MCM-41 and sulfonic modified MCM-41. Surface silanols groups, as well as the physically adsorbed water, resulted in the wide peak near 3,463 cm^{-1}. A deformational vibration of adsorption water led to the peak at 1,635 cm^{-1}. The asymmetric, symmetric

extending, and bending vibration of Si–O–Si groups are responsible for the typical peaks at 1,084; 799; and 458 cm^{-1}, correspondingly [24]. The characteristic peak at 965 cm^{-1} represents the stretching vibrations of surface Si–O^- groups [25]. Moreover, the asymmetric stretching vibrations of the Si–O–Si bridges lead to the peak at 1,239 cm^{-1}. The adsorption peak of S=O groups at 1,140 cm^{-1} is covered by the peaks at 1,239 and 1084 cm^{-1}, and therefore a wide peak between 1,084 and 1,239 cm^{-1} appears. This was also reported elsewhere [26].

The EDS test results are shown in Fig. 2 and quantitative information is exhibited in Table 1. It can be observed that sulfur has been detected in sulfonic modified MCM-41. In agreement with FT-IR results, sulfonic groups have been successfully grafted onto MCM-41.

Fig. 3 shows the TGA of MCM-41 and S-MCM-41. It indicates the grafting amount of sulfonic acid groups onto MCM-41. At the initial stage, physically adsorbed water is vaporized from the materials. This stage occurs at around 23°C–120°C. Then, the loss of grafted sulfonic groups is exhibited from 120°C to 600°C. The mass loss in this process is 14.14%. However, MCM-41 experiences a mass loss of 4.78% after 120°C. Considering some silanol groups were cost because of the silica silanization reaction, this mass loss can be attributed to the water consumption during the condensation of the remaining silanol groups [13].

To investigate the properties and features of MCM-41 and S-MCM-41, XRD was used to study the structure of the mesoporous products. Fig. 4 shows the powder XRD results of MCM-41 and S-MCM-41. It could be observed that four typical diffraction peaks in the XRD patterns of MCM-41: a noticeable peak of (100) planes and three weaker peaks of (110), (200), and (210). This result

Table 1
Quantitative analysis of elements in sulfonic modified MCM-41

Sample	Elements present (wt.%)		
	Si	O	S
S-MCM-41	39.65	57.50	2.85

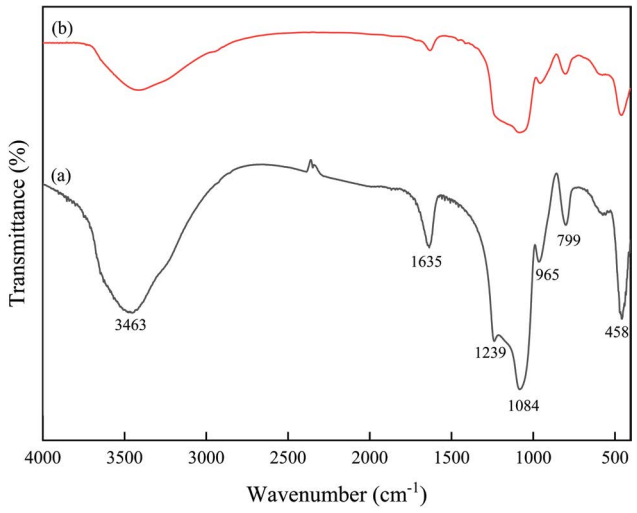

Fig. 1. FT-IR spectra of (a) MCM-41 and (b) modified MCM-41.

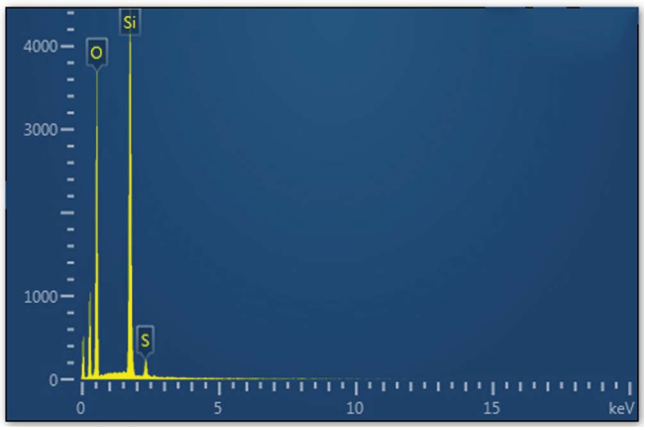

Fig. 2. EDS spectra of sulfonic modified MCM-41.

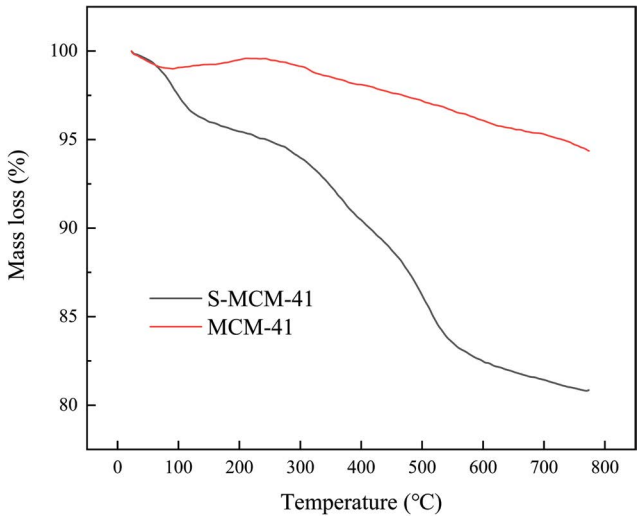

Fig. 3. TG analysis of MCM-41 and S-MCM-41.

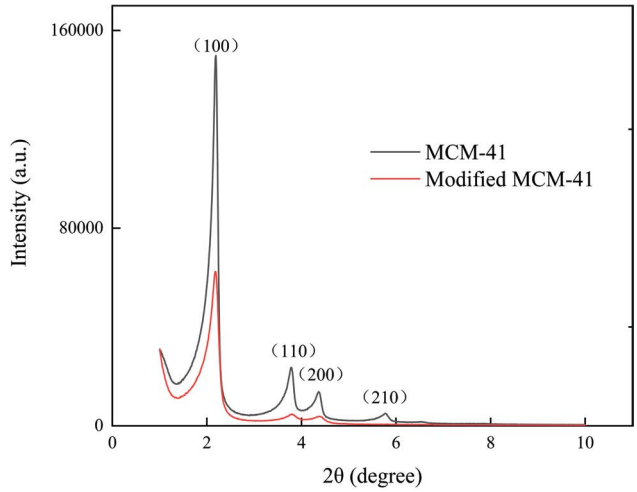

Fig. 4. XRD image of MCM-41 and modified MCM-41.

suggested the representative 2D hexagonal arrays construction of MCM-41 [27]. In the XRD result of S-MCM-41, however, the intensity of characteristic peaks became weaker and the (210) peak has not existed. This means the modification has an adverse impact on the long-range ordered structure of the material, but S-MCM-41 still possesses an ordered 2D hexagonal structure. In different studies [16, 27, 28], the modification processes can lead to different levels of the collapse of ordered structures in mesoporous materials. Different functional groups or compounds and different modification methods may be responsible for the various damage of the structure.

Through SEM and TEM, the surface morphology and pore structure can be observed directly. SEM pictures of the MCM-41 and S-MCM-41 are presented in Fig. 5a and b. MCM-41 has a rod shape and after modification, the shape was not changed much. The Supplementary information about the pore structure in the MCM-41 and S-MCM-41 was explored by TEM, as seen in Fig. 5c and d. The TEM images presented the lamellar structure as well as the 2D hexagonal arrangements of pore shape which both belong to typical MCM-41 materials. Moreover, the ordered structure did not see distortion after the grafting of sulfonic groups.

Normally, XRD, TEM, and N_2 adsorption–desorption are the fundamental technologies to determine the successfully synthesized mesoporous silica. N_2 adsorption–desorption was used in the present study to investigate the pore parameters of MCM-41 and S-MCM-41. Fig. 6 presents the nitrogen adsorption–desorption isotherms of MCM-41 and S-MCM-41. Both MCM-41 materials show type IV isotherms, which corresponds to the representative result of MCM-41. At low relative pressure, the monolayer/multilayer uptake on the pore walls leads to steady growth in gas absorption [29]. The volume adsorbed of the adsorption isotherms soared dramatically between 0.20 and 0.40 (P/P_0). The capillary condensation caused this jump, and it was associated with uniform mesopores. A hysteresis loop showed up in this image because the desorption route did not follow the same way of adsorption. The outline and

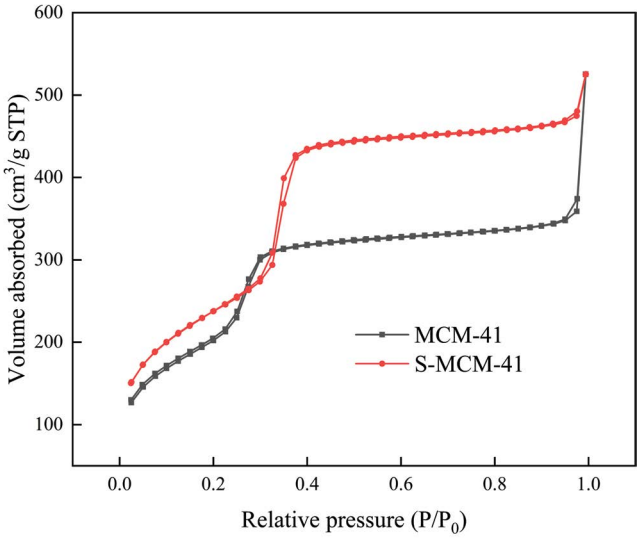

Fig. 6. N_2 adsorption–desorption isotherms of MCM-41 and S-MCM-41.

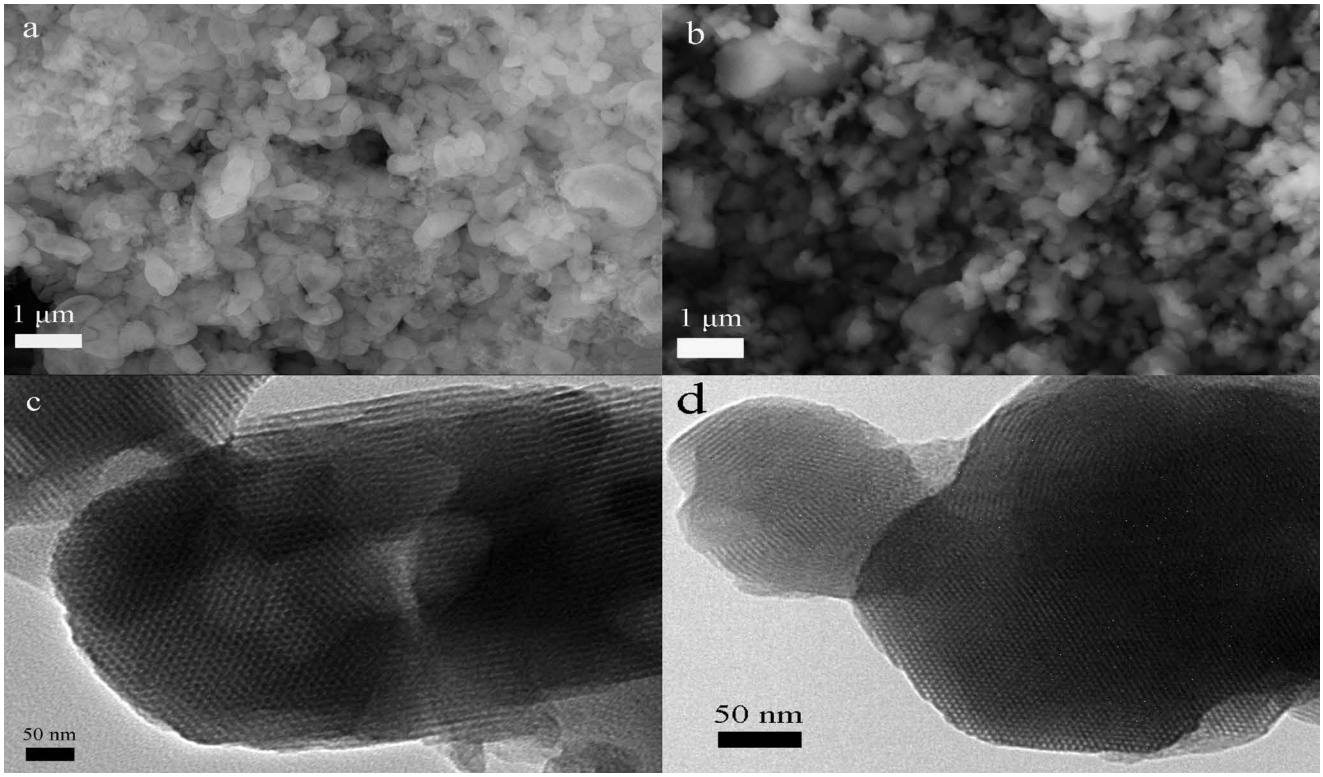

Fig. 5. SEM of (a) MCM-41, (b) S-MCM-41 and TEM of (c) MCM-41, (d) S-MCM-41.

the volume of the pores as well as the connectivity could be investigated by the shape of this loop [30]. The hysteresis loop in Fig. 6 was attributed to the slit-shaped pores in MCM-41 and S-MCM-41. The sharp growth of the capillary condensation step suggests that the MCM-41 and S-MCM-41 have quite uniform pore sizes [31]. The multilayer uptake on the outside surface of the materials contributed to the plateau with a slight inclination from 0.35 to 0.95 of relative pressure (P/P_0). The remained available pores are responsible for a sharp rise of the isotherms curve when the relative pressure reached the maximum [32]. However, the additional strain in the grafting process leads to a slight change in the shape of the isotherms [16]. Furthermore, the Brunauer-Emmett-Teller (BET) surface area, pore diameters, and total pore volume can be seen in Table 2. The surface area and pore sizes decrease slightly after the modification because the functional groups occupy some space on the surface and in the pores of the materials. But the changes are slight and the modified mesoporous materials still possess large pores and surface area.

After all of the characterization, slight changes can be seen after the modification of MCM-41. But S-MCM-41 still has highly ordered 2D hexagonal pore structures and large pore sizes.

3.2. Adsorption studies

3.2.1. Effect of the pH

Among all the factors in the adsorption experiments, the initial pH values of the MB solution may have the most noticeable impact on the adsorption capacity of absorbents. The effect of pH on the adsorption process was studied when the initial concentration of MB is 500 mg/L, the absorbent dose is 1.0 g/L, the contact time is 60 min, and the temperature is 30°C. As shown in Fig. 7, the performance of MCM-41 increased with the growth of initial pH values between 2 and 10, and the adsorption of MB on S-MCM-41 improved when the pH values vary from 2 to 11. MB is classified as a cationic dye and Fig. 8 indicates that sulfonic modified MCM-41 is positively charged when the pH value is lower than 3.5 [26]. Because deprotonation of sulfonic acid groups is starting when the pH value reaches 3.5. This led to the proliferation of MB adsorption on S-MCM-41 when pH values increased from 3 to 4. Therefore, the increasing Q_e can be attributed to the falling negative charge density of mesoporous adsorbents with the growth of initial pH values in MB solution. The adsorption sites on the adsorbents can be partly occupied by H^+ in the acidic environment [33]. After the pH values of MB solution exceed 11, Q_e dropped significantly. This represents the release of absorbed dye molecules from S-MCM-41 because of the hydrolysis of those dye molecules by OH^- in the alkalic environment [34]. Considering the initial pH of the MB solution is around 5, the potential of S-MCM-41 cannot be fully discovered under this circumstance. In this case, all the following adsorption experiments were carried on in the MB solution with an initial pH of 11. In this case, all the following adsorption experiments were carried on in the MB solution with an initial pH of 10. The Q_e on MCM-41 at pH value of 11 is 463.23 mg/g while the Q_e on S-MCM-41 is 593.22 mg/g under the same circumstance. Therefore, the modification of grafting sulfonic acid groups can significantly improve the adsorption of cationic dyes on MCM-41 adsorbents. The adsorption mechanism of S-MCM-41 for cationic dyes is the electrostatic attraction between negatively charged adsorbents and positively charged dye molecules.

Table 2
Pore parameters of MCM-41 and S-MCM-41

Materials	BET surface area (m^2/g)	Pore diameters (nm)	Pore volume (cm^3/g)
MCM-41	1,145.960	3.135	0.348
S-MCM-41	843.696	2.969	0.300

3.2.2. Effect of the adsorbent–adsorbate ratio

The effect of the adsorbent-adsorbate ratio (S-MCM-41/MB solution) was explored at 30°C for 60 min, and the initial

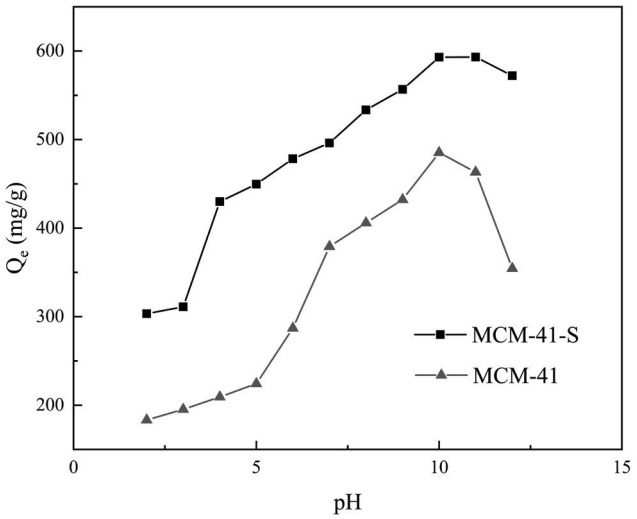

Fig. 7. Effect of pH on the adsorption of MB.

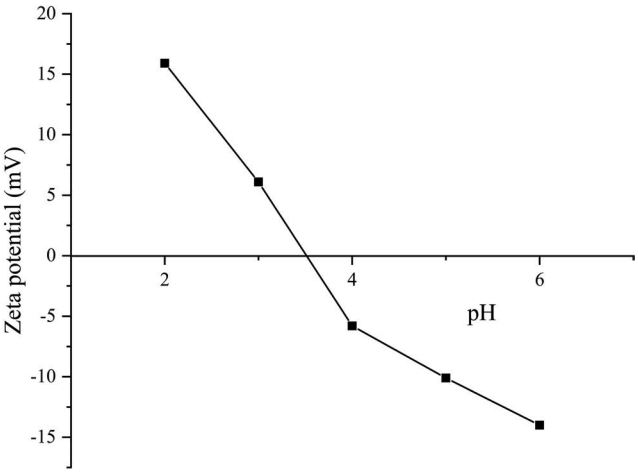

Fig. 8. Effect of pH on zeta potential of S-MCM-41.

concentration of the cationic dye solution was 500 mg/L. As shown in Fig. 9, the percentage of MB removal (A%) increased significantly when the dose of adsorbent saw an increment from 0.5 to 1.0 g/L. Higher surface area, more pores, and functional groups are offered when more S-MCM-41 are used [35,36]. This will cause more available adsorption sites for MB molecules. However, when the dose of S-MCM-41 exceeded 1.0 g/L, the improvement in A% was extremely limited. Meanwhile, Q_e showed a steady decrease which can be attributed to the competitive adsorption on the available adsorption sites [37]. Therefore, in the following adsorption experiments, 1 g/L S-MCM-41 was used as the adsorbent.

3.2.3. Adsorption time and kinetics

To observe the effectiveness of this adsorbent on different adsorption times, experiments were carried on at 30°C, and the concentration of MB solution was 500 mg/L. As presented in Fig. 10, Q_e increased noticeably during the first 10 min, and it took another 30 min to reach the adsorption equilibrium gradually. Electrostatic attraction between the negatively charged surface of S-MCM-41 and the cationic dye leads to rapid adsorption at the beginning stage [38]. Furthermore, the adsorption capacities remained almost unchanged when the contact time was from 40 to 90 min, because most of the adsorption sites on S-MCM-41 were taken by MB molecules.

To explore the mechanism of adsorption, an adsorption kinetics study was carried on including pseudo-first-order [39] and pseudo-second-order [40]. When the adsorption reaches a balance between S-MCM-41 and MB molecules, the reaction can be considered as invertible. The rate constants k_1 and k_2 can be obtained by subsequent procedure:

$$\frac{dQ}{dt} = k_1\left(Q_e - Q\right)\left[\text{pseudo-first-order equation}\right] \tag{3}$$

$$\frac{dQ}{dt} = k_2\left(Q_e - Q\right)^2\left[\text{pseudo-second-order equation}\right] \tag{4}$$

where Q_e and Q are the adsorption quantity (mg/g) at balance and any time t (min); k_1 (min^{-1}) and k_2 (g/mg min) represent the adsorption rate constants for pseudo-first-order and pseudo-second-order models. After making boundary amount $Q = 0$ when $t = 0$ and $Q = Q_t$ when $t = t$. Eqs. (3) and (4) can be transformed to:

$$Q_t = Q_e\left[1 - \exp\left(-k_1 t\right)\right] \tag{5}$$

$$Q_t = \frac{Q_e^2 k_2 t}{\left(1 + Q_e k_2 t\right)} \tag{6}$$

Fig. 10 indicates the image of pseudo-first-order and pseudo-second-order kinetic models for the adsorption of dye molecules on S-MCM-41. As shown in Table 3, the linear regression coefficient (R^2) and kinetic constants are calculated and listed. The results exhibit a good fit in pseudo-first-order kinetic model according to the values of R^2 (0.994 for pseudo-first-order and 0.891 for pseudo-second-order).

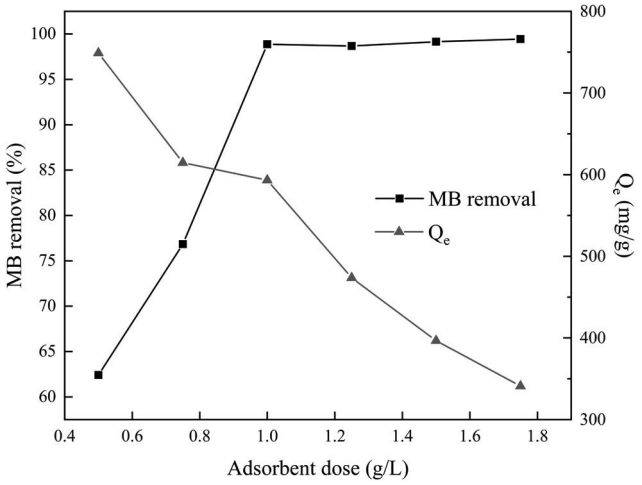

Fig. 9. Effect of S-MCM-41 dose on MB removal.

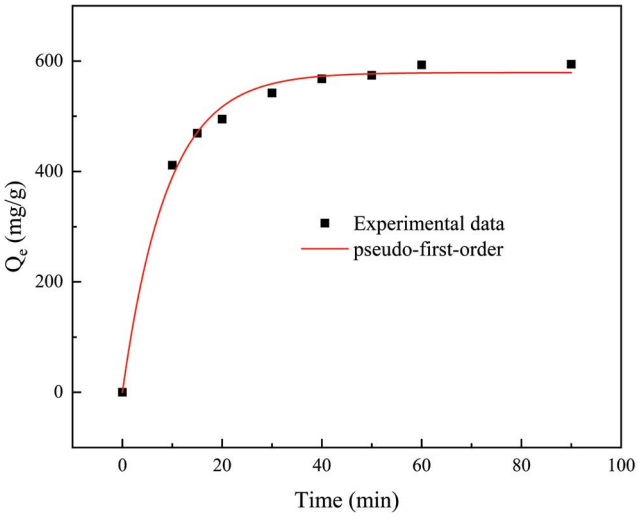

Fig. 10. Adsorption kinetics of MB on S-MCM-41.

Table 3
Kinetic parameters for removal of MB by S-MCM-41

C_0 (mg/L)	Q_e (mg/g)	Pseudo-first-order			Pseudo-second-order		
		Q_c (mg/g)	k_1 (min^{-1})	R^2	Q_c (mg/g)	k_2 (g/mg min)	R^2
500	594.23	579.08	0.112	0.994	530.86	–2.903	0.891

Furthermore, the calculated adsorption quantity Q_c in both kinetic models fit the experimental data of Q_e, and it shows a better fit in the pseudo-first-order kinetic model. Therefore, the adsorption behavior of MB molecules on S-MCM-41 can be better explained by a pseudo-first-order kinetic model.

3.2.4. Adsorption isotherms

The interactive behavior between MB molecules and S-MCM-41 can be revealed by an equilibrium adsorption isotherm which is the essential part of the design of adsorption systems. The most common isotherm model was used to deal with the experimental data. Langmuir isotherm indicates that monolayer adsorption is performed on the same sites in the adsorption process [41]. If no extra adsorption is performed, it will be considered as the limitation of this process. The Langmuir isotherm model is given as follows:

$$Q_e = \frac{Q_{\max} K_L C_e}{\left(1 + K_L C_e\right)} \tag{7}$$

where $Q_{\max}$ (mg/g) is the maximum adsorption capacity of the dye on BW-MCM-41; C_e (mg/L) stands for the balanced concentration of MB solution; K_L (L/mg) represents the Langmuir constant. R_L represents the separation factor which is employed to identify if the adsorption is favorable. The dimensionless constant R_L is described as follows [42]:

$$R_L = \frac{1}{\left(1 + K_L C_0\right)} \tag{8}$$

With different values of R_L, the adsorption behaviors are different: (1) irreversible as $R_L = 0$; (2) favorable ($0 < R_L < 1$); (3) linear as $R_L = 1$; (4) unfavorable ($R_L > 1$).

Fig. 11 shows the results of Langmuir fitting with the experimental data of MB on S-MCM-41. Table 4 lists the Langmuir constant and important coefficient for the isotherm model. According to the R^2, the adsorption behavior of MB molecules on S-MCM-41 fits well with the Langmuir isotherm model. The monolayer coverage of the dye molecules on the outside and inside of S-MCM-41 is demonstrated by the well-fitting with Langmuir isotherm [43]. The calculated adsorption capacity $Q_{\max}$ is 665.92 mg/g, which fits well with the experimental data. Furthermore, the adsorption of MB on S-MCM-41 can be considered favorable because R_L is 0.0012.

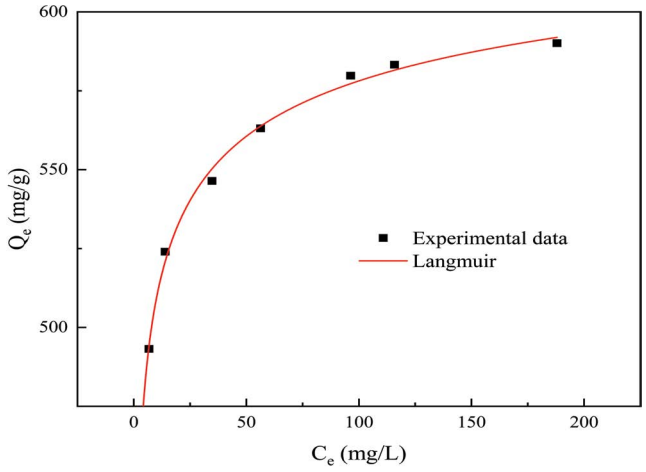

Fig. 11. Adsorption isotherm of S-MCM-41.

3.2.5. Adsorption thermodynamics

Thermodynamic parameters including the Gibbs free energy change $\Delta G°$, enthalpy change $\Delta H°$, and entropy change ΔS^0 are used to study the influence of heat on the removal of MB by BW-MCM-41. They can be calculated by Eqs. (9)–(11):

$$\Delta G° = -RT \ln K_0 \tag{9}$$

$$K_0 = \frac{Q_e}{C_e} \tag{10}$$

$$\ln K_0 = \frac{\Delta S°}{R} - \frac{\Delta H°}{RT} \tag{11}$$

where R is the gas constant (8.314 J/mol K); K_0 represents the distribution coefficient; T (K) stands for the temperature of the adsorbate.

A linear plot of $\ln K_0$ vs. $1/T$ is drawn to calculate $\Delta H°$ and $\Delta S°$ from the slope and intercept, respectively. Both of them and $\Delta G°$ are shown in Table 5. It can be observed that $\Delta G° < 0$ when the temperatures vary from 20°C to 40°C, which means the adsorption process is unprompted. It indicates the strong attraction between MB molecules and S-MCM-41. Furthermore, physisorption can cause $\Delta G°$ to vary between –20 and 0 kJ/mol while chemisorption leads to the range of –400 to –80 kJ/mol [44]. As a result, this adsorption process can be defined as physisorption. The removal of MB can be acknowledged as physisorption because of the absolute magnitude $\Delta H° > 40$ kJ/mol,

Table 4
Langmuir parameters for MB on S-MCM-41

Temperature (°C)	30
$Q_{\max}$ (mg/g)	665.92
K_L (L/mg)	1.60
R_L	0.0012
R^2	0.995

Table 5
Thermodynamic parameters of the adsorption of MB on S-MCM-41

	$\Delta G°$ (kJ/mol)	$\Delta H°$ (kJ/mol)	$\Delta S°$ (J/K mol)
20°C	–3.687	103.770	387.224
30°C	–10.801		
40°C	–11.431		

which is in agreement with the analysis above. The positive value of $\Delta H°$ suggests the removal process is endothermic. Considering the adsorption process of MB on S-MCM-41 is physisorption, it will not absorb heat. Therefore, this phenomenon might be attributed to the decomposition of some MB in the solution, because MB can be photodegraded [45–47]. Moreover, according to the second law of thermodynamics, any change in an isolated system will lead to entropy production, which can be demonstrated by the calculated result of $\Delta S°$. Higher Q_e at higher temperature indicates the removal of MB by S-MCM-41 more favorable at high temperature because H^+ are more active at higher temperature and this leads to more SO_3^- for MB adsorption.

3.2.6. Characterization of S-MCM-41 after adsorption

A series of characterization methods were used to observe the change of S-MCM-41 after adsorption. As shown in Fig. 12, the intensity of peaks at 1,213; 965; and 799 cm^{-1} significantly diminished, because MB was adsorbed on S-MCM-41 by the sulfonic acid groups and the surface Si–O^- and Si–O–Si groups [48]. As seen in Fig. 13, the surface of S-MCM-41 was covered by MB molecules. After the desorption of MB, the morphology of S-MCM-41 also recovered. Fig. 14 indicates that the peak of N1s increased after adsorption because of the nitrogen in MB. This suggests MB molecules were adsorbed on S-MCM-41. The pore parameters and surface area of S-MCM-41 in the adsorption and regeneration process have been listed in Table 6. MB molecules occupied a large part of surface area and adsorption sites. Most adsorption sites can be recovered after the desorption of MB.

3.2.7. Regeneration of S-MCM-41

The recycling ability of adsorbents is extremely important to practical application. S-MCM-41 was recovered by washing with HCl solution and continued to adsorb MB. As shown in Fig. 15, S-MCM-41 exhibits high adsorption capacity to MB after five cycles, although Q_e decreased slightly after four-times regeneration. Therefore, BW-MCM-41 is an excellent adsorbent for MB and can be easily regenerated.

4. Conclusions

The present study suggests sulfonic modified MCM-41 is a promising adsorbent for cationic dye removal. FT-IR and EDS show sulfonic acid groups are successfully grafted onto MCM-41. XRD, SEM, TEM, and N_2 adsorption and desorption results suggest S-MCM-41 still possess highly ordered 2D hexagonal pore structure, high surface area, and large pore size. The Q_e on MCM-41 at pH value of 11 is 463.23 mg/g while the Q_e on S-MCM-41 is 593.22 mg/g under the same circumstance. The adsorption performance of S-MCM-41 is the best at a pH value of 11 and an adsorbent dose of 1.0 g/L. The pseudo-first-order kinetic model

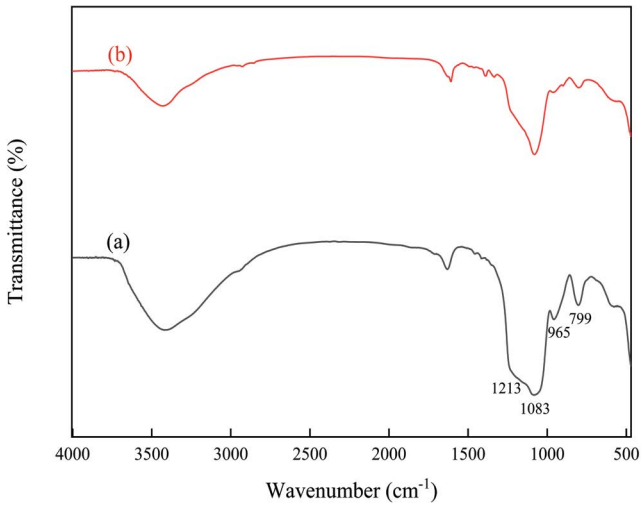

Fig. 12. FT-IR results of S-MCM-41 before (a) and after (b) adsorption.

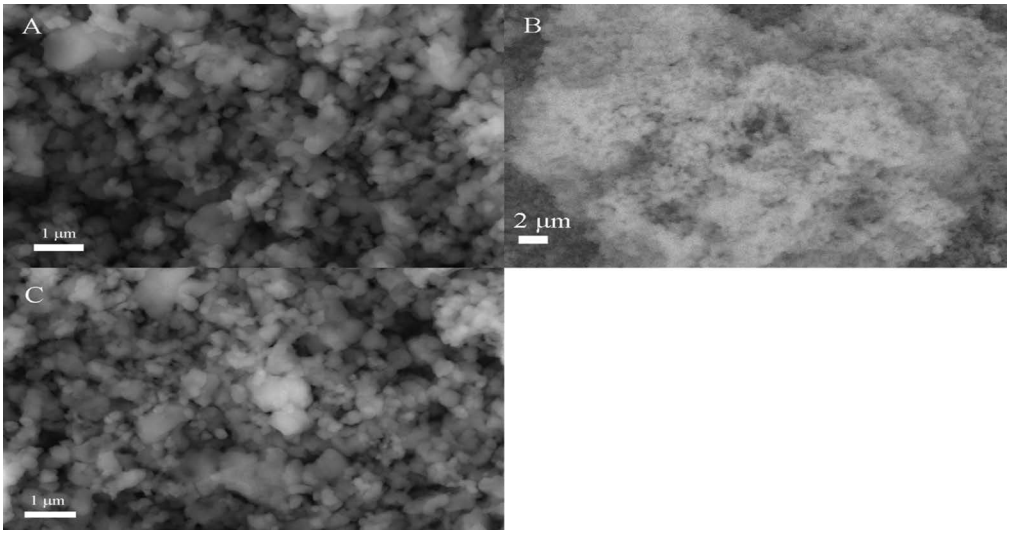

Fig. 13. SEM images of S-MCM-41 before (A), after (B) adsorption, and after regeneration (C).

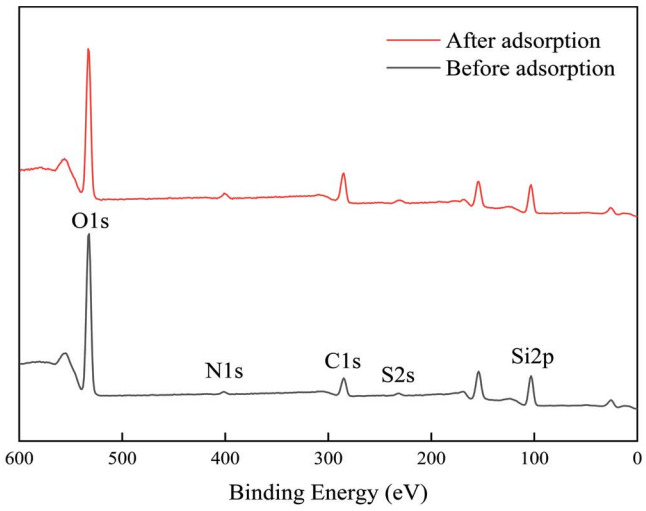

Fig. 14. XPS image of S-MCM-41 before and after adsorption.

Table 6
Pore parameters of S-MCM-41 before, after adsorption, and after regeneration

S-MCM-41	BET surface area (m^2/g)	Pore diameters (nm)	Pore volume (cm^3/g)
Before adsorption	843.696	2.969	0.300
After adsorption	487.907	1.675	0.193
After regeneration	829.715	2.721	0.287

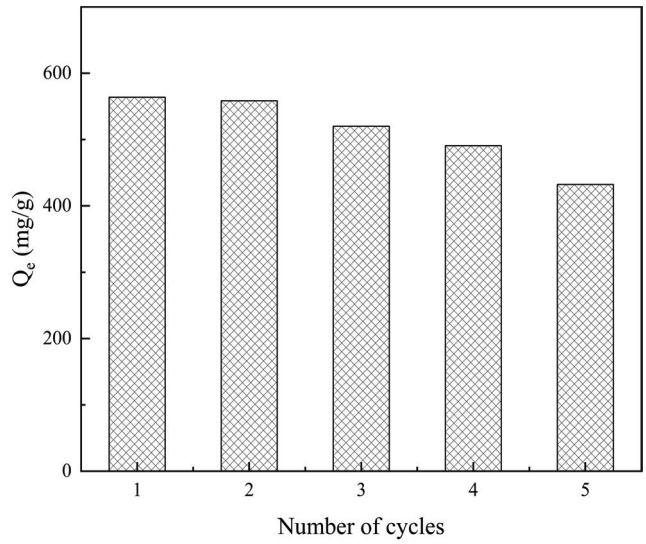

Fig. 15. Performance for recovered S-MCM-41.

can explain the adsorption process better, and it is well-fitted with the Langmuir isotherm model. The adsorption of MB is a physical process and it is more favorable at high temperatures. Moreover, S-MCM-41 can be easily recovered and still possess high adsorption capacity after five cycles.

Acknowledgments

The authors want to thank Prof. Haibo Li, Prof. Yinghua Li, and Prof. Xi Chen for providing their equipment.

References

[1] Y. Shao, X. Wang, Y. Kang, Y. Shu, Q. Sun, L. Li, Application of Mn/MCM-41 as an adsorbent to remove methyl blue from aqueous solution, J. Colloid Interface Sci., 429 (2014) 25–33.
[2] M. Arulkumar, P. Sathishkumar, T. Palvannan, Optimization of Orange G dye adsorption by activated carbon of *Thespesia populnea* pods using response surface methodology, J. Hazard. Mater., 186 (2011) 827–834.
[3] C. Park, M. Lee, B. Lee, S.W. Kim, H.A. Chase, J. Lee, S. Kim, Biodegradation and biosorption for decolorization of synthetic dyes by *Funalia trogii*, Biochem. Eng. J., 36 (2007) 59–65.
[4] M. Naushad, A.A. Alqadami, Z.A. AlOthman, I.H. Alsohaimi, M.S. Algamdi, A.M. Aldawsari, Adsorption kinetics, isotherm and reusability studies for the removal of cationic dye from aqueous medium using arginine modified activated carbon, J. Mol. Liq., 293 (2019) 111442–111449, doi: 10.1016/j.molliq.2019.111442.
[5] M. Khodaie, N. Ghasemi, B. Moradi, M. Rahimi, Removal of Methylene Blue from wastewater by adsorption onto $ZnCl_2$ activated corn husk carbon equilibrium studies, J. Chem., 2013 (2013) 383985–383990, doi: 10.1155/2013/383985.
[6] T. Anitha, P. Senthil Kumar, K. Sathish Kumar, Synthesis of nano-sized chitosan blended polyvinyl alcohol for the removal of Eosin Yellow dye from aqueous solution, J. Water Process Eng., 13 (2016) 127–136.
[7] S. Debnath, N. Ballav, A. Maity, K. Pillay, Single stage batch adsorber design for efficient Eosin yellow removal by polyaniline coated ligno-cellulose, Int. J. Biol. Macromol., 72 (2015) 732–739.
[8] C.H. Huang, K.P. Chang, H.D. Ou, Y.C. Chiang, C.F. Wang, Adsorption of cationic dyes onto mesoporous silica, Microporous Mesoporous Mater., 141 (2011) 102–109.
[9] A. Namane, A. Mekarzia, K. Benrachedi, N.B. Bensemra, A. Hellal, Determination of the adsorption capacity of activated carbon made from coffee grounds by chemical activation with $ZnCl_2$ and H_3PO_4, J. Hazard. Mater., 119 (2005) 189–194.
[10] E. Forgacs, T. Cserhati, G. Oros, Removal of synthetic dyes from wastewaters: a review, Environ. Int., 30 (2004) 953–971.
[11] P.V. Messina, P.C. Schulz, Adsorption of reactive dyes on titania-silica mesoporous materials, J. Colloid Interface Sci., 299 (2006) 305–320.
[12] S. Wang, Z.H. Zhu, Characterisation and environmental application of an Australian natural zeolite for basic dye removal from aqueous solution, J. Hazard. Mater., 136 (2006) 946–952.
[13] A.R. Cestari, E.F. Vieira, G.S. Vieira, L.E. Almeida, Aggregation and adsorption of reactive dyes in the presence of an anionic surfactant on mesoporous aminopropyl silica, J. Colloid Interface Sci., 309 (2007) 402–411.
[14] T.A. Germi, A. Nematollahzadeh, Bimodal porous silica microspheres decorated with polydopamine nano-particles for the adsorption of methylene blue in fixed-bed columns, J. Colloid Interface Sci., 470 (2016) 172–182.
[15] S. Ahmed, A. Ramli, S. Yusup, M. Farooq, Adsorption behavior of tetraethylenepentamine-functionalized Si-MCM-41 for CO_2 adsorption, Chem. Eng. Res. Des., 122 (2017) 33–42.
[16] A. Sharma, A. Dubey, Surface modified mesoporous silica polymer nanocomposites for adsorption of dyes from aqueous solution, J. Porous Mater., 24 (2016) 429–435.
[17] A.G.S. Prado, B.S. Miranda, G.V.M. Jacintho, Interaction of indigo carmine dye with silica modified with humic acids at solid/liquid interface, Surf. Sci., 542 (2003) 276–282.
[18] S. Ray, M. Takafuji, H. Ihara, Peptide-based surface modified silica particles: adsorption materials for dye-loaded wastewater treatment, RSC Adv., 3 (2013) 23664–23672.
[19] Z. Liang, Z. Zhao, T. Sun, W. Shi, F. Cui, Enhanced adsorption of the cationic dyes in the spherical CuO/meso-silica nano

composite and impact of solution chemistry, J. Colloid Interface Sci., 485 (2017) 192–200.
[20] M.K. Oden, S. Kucukcongar, Acid and ultrasound assisted modification of boron enrichment process waste and using for methylene blue removal from aqueous solutions, Global Nest J., 20 (2018) 234–242.
[21] S.H. Lee, S.S. Park, S. Parambadath, C.S. Ha, Sulphonic acid functionalized periodic mesoporous organosilica with the bridged bissilylated urea groups for high selective adsorption of cobalt ion from artificial seawater, Microporous Mesoporous Mater., 226 (2016) 179–190.
[22] M. Goswami, P. Phukan, Enhanced adsorption of cationic dyes using sulfonic acid modified activated carbon, J. Environ. Chem. Eng., 5 (2017) 3508–3517.
[23] M. Bandyopadhyay, N. Tsunoji, R. Bandyopadhyay, T. Sano, Comparison of sulfonic acid loaded mesoporous silica in transesterification of triacetin, React. Kinet. Mech. Catal., 126 (2018) 167–179.
[24] A. Heidari, H. Younesi, Z. Mehraban, Removal of Ni(II), Cd(II), and Pb(II) from a ternary aqueous solution by amino functionalized mesoporous and nano mesoporous silica, Chem. Eng. J., 153 (2009) 70–79.
[25] R. Takahashi, S. Sato, T. Sodesawa, M. Kawakita, K. Ogura, High surface-area silica with controlled pore size prepared from nanocomposite of silica and citric acid, J. Phys. Chem. B, 104 (2000) 12184–12191.
[26] L. Zhang, G. Zhang, S. Wang, J. Peng, W. Cui, Sulfoethyl functionalized silica nanoparticle as an adsorbent to selectively adsorb silver ions from aqueous solutions, J. Taiwan Inst. Chem. Eng., 71 (2017) 330–337.
[27] X. Jia, X. He, K. Han, Y. Ba, X. Zhao, Q. Zhang, La_2O_3-modified MCM-41 for efficient phosphate removal synthesized using natural diatomite as precursor, Water Sci. Technol., 79 (2019) 1878–1886.
[28] M. Anbia, S.A. Hariri, S.N. Ashrafizadeh, Adsorptive removal of anionic dyes by modified nanoporous silica SBA-3, Appl. Surf. Sci., 256 (2010) 3228–3233.
[29] K.S. Hui, C.Y. Chao, Synthesis of MCM-41 from coal fly ash by a green approach: influence of synthesis pH, J. Hazard. Mater., 137 (2006) 1135–1148.
[30] V. Meynen, P. Cool, E.F. Vansant, Verified syntheses of mesoporous materials, Microporous Mesoporous Mater., 125 (2009) 170–223.
[31] H. Yu, X. Xue, D. Huang, Synthesis of mesoporous silica materials (MCM-41) from iron ore tailings, Mater. Res. Bull., 44 (2009) 2112–2115.
[32] A.C. Voegtlin, A. Matijasic, J. Patarin, C. Sauerland, Y. Grillet, L. Huve, Room-temperature synthesis of silicate mesoporous MCM-41-type materials: influence of the synthesis pH on the porosity of the materials obtained, Microporous Mater., 10 (1997) 137–147.
[33] M. Rafatullah, O. Sulaiman, R. Hashim, A. Ahmad, Adsorption of methylene blue on low-cost adsorbents: a review, J. Hazard. Mater., 177 (2010) 70–80.
[34] Z.H. Yu, S.R. Zhai, H. Guo, T.M. lv, Y. Song, F. Zhang, H.C. Ma, Removal of methylene blue over low-cost mesoporous silica nanoparticles prepared with naturally occurring diatomite, J. Sol-Gel Sci. Technol., 88 (2018) 541–550.
[35] D.A. Fungaro, M. Bruno, L.C. Grosche, Adsorption and kinetic studies of methylene blue on zeolite synthesized from fly ash, Desal. Water Treat., 2 (2009) 231–239.
[36] K.G. Bhattacharyya, A. Sharma, Adsorption of Pb(II) from aqueous solution by *Azadirachta indica* (Neem) leaf powder, J. Hazard. Mater., 113 (2004) 97–109.
[37] H. Guo, S.F. Zhang, Z.N. Kou, S.R. Zhai, W. Ma, Y. Yang, Removal of cadmium(II) from aqueous solutions by chemically modified maize straw, Carbohydr. Polym., 115 (2015) 177–185.
[38] K. Rida, S. Bouraoui, S. Hadnine, Adsorption of methylene blue from aqueous solution by kaolin and zeolite, Appl. Clay Sci., 83–84 (2013) 99–105.
[39] Y.S. Ho, Citation review of Lagergren kinetic rate equation on adsorption reactions, Scientometrics, 59 (2004) 171–177.
[40] Y.S. Ho, G. McKay, Sorption of dye from aqueous solution by peat, Chem. Eng. J., 70 (1998) 115–124.
[41] I. Langmuir, The constitution and fundamental properties of solids and liquids. II. Liquids, J. Am. Chem. Soc., 39 (1917) 1848–1906.
[42] G. McKay, Adsorption of dyestuffs from aqueous solutions with activated carbon – 1. Equilibrium and batch contact-time studies, J. Chem. Technol. Biotechnol., 32 (1982) 759–772.
[43] L. Lin, S.R. Zhai, Z.Y. Xiao, Y. Song, Q.D. An, X.W. Song, Dye adsorption of mesoporous activated carbons produced from NaOH-pretreated rice husks, Bioresour. Technol., 136 (2013) 437–443.
[44] D. Karadag, M. Turan, E. Akgul, S. Tok, A. Faki, Adsorption equilibrium and kinetics of Reactive Black 5 and Reactive Red 239 in aqueous solution onto surfactant-modified zeolite, J. Chem. Eng. Data, 52 (2007) 1615–1620.
[45] Z.U.H. Khan, A. Khan, Y. Chen, A.u. Khan, N.S. Shah, N. Muhammad, B. Murtaza, K. Tahir, F.U. Khan, P. Wan, Photo catalytic applications of gold nanoparticles synthesized by green route and electrochemical degradation of phenolic Azo dyes using AuNPs/GC as modified paste electrode, J. Alloys Compd., 725 (2017) 869–876.
[46] M. Naushad, G. Sharma, Z.A. Alothman, Photodegradation of toxic dye using Gum Arabic-crosslinked-poly(acrylamide)/$Ni(OH)_2$/FeOOH nanocomposites hydrogel, J. Cleaner Prod., 241 (2019) 118263–118271, doi: 10.1016/j.jclepro.2019.118263.
[47] G. Sharma, D.D. Dionysiou, S. Sharma, A. Kumar, A.a.H. Al-Muhtaseb, M. Naushad, F.J. Stadler, Highly efficient Sr/Ce/activated carbon bimetallic nanocomposite for photoinduced degradation of rhodamine B, Catal. Today, 335 (2019) 437–451.
[48] L. Zhang, H. Zhang, W. Guo, Y. Tian, Removal of malachite green and crystal violet cationic dyes from aqueous solution using activated sintering process red mud, Appl. Clay Sci., 93–94 (2014) 85–93.